IEEE Open Journal of
Intelligent Transportation
Systems

Received 13 July 2024; revised 12 October 2024; accepted 3 November 2024. Date of publication 5 November 2024; date of current version 22 November 2024.

Digital Object Identifier 10.1109/OJITS.2024.3492115

Control Allocation Approach Using Differential Steering to Compensate for Steering Actuator Failure

ALEXANDER SEIFFER[1], MICHAEL FREY[2], AND FRANK GAUTERIN[2]

[1]SHARE at KIT, Schaeffler Technologies AG & Co. KG., 76131 Karlsruhe, Germany
[2]Institute of Vehicle System Technology, Karlsruhe Institute of Technology, 76131 Karlsruhe, Germany

CORRESPONDING AUTHOR: A. SEIFFER (e-mail: alexander.seiffer@schaeffler.com)

This work was supported by the KIT Publication Fund of the Karlsruhe Institute of Technology.

ABSTRACT Wheel-selective drives on the steered axle of a vehicle with Ackermann steering allow for the generation of steering torque without the use of a steering actuator. If different drive torques are applied to the left and right driven wheels, their effect on the steering torque is not balanced, and a resulting steering torque remains (differential steering). Thus, the function of a steering actuator can be replaced, e.g., in case of a failure. Previous studies have demonstrated the effectiveness of controlling a vehicle using differential steering. However, the vehicle dynamics during the failure-induced transition from actuator-based to differential steering control have not been thoroughly investigated. In this work, we utilize a cascaded vehicle dynamics control approach with control allocation to distribute the total drive and steering torques to the available actuators in an overactuated chassis system. Based on both simulation studies and validation experiments with a demonstrator vehicle, we investigate the vehicle dynamics immediately following actuator failures. Our cascaded approach ensures precise vehicle guidance in both nominal and redundancy mode via differential steering. After a sudden actuator failure, vehicle guidance is reliably maintained, even in dynamic driving conditions, as the approach also considers the effect of drive torque distribution on the total yaw torque (torque vectoring). The analyses conducted using the proposed approach demonstrate that a safe transition to cross-actuator functional redundancy after an actuator failure is achievable. Consequently, differential steering can be evaluated as a suitable basis for cross-actuator functional redundancy concepts to enable fault-tolerant operation of steer-by-wire systems.

INDEX TERMS Chassis control, control allocation, differential steering, drive-by-wire, fault tolerance, over-actuated vehicle, redundancy, resilience, steer-by-wire, torque steer, torque vectoring, vehicle dynamics control, wheel-individual drive.

I. INTRODUCTION

AUTOMATED driving in passenger cars is on the rise as the capabilities of driver assistance systems continue to improve. In addition, automated driving and driverless vehicles are increasingly being used in other vehicle classes, such as commercial vehicles, public transportation, and automated ground vehicles.

In conventionally steered vehicles, the driver can take control of the vehicle at any time by turning the steering wheel, even if, for example, the power steering fails [1]. The reliance on the driver as a safe fallback for lateral control is eliminated if the vehicle is equipped with steer-by-wire technology, which lacks a mechanical linkage between the steering wheel and the suspension. This also applies to vehicles that allow the driver to temporarily or permanently transfer responsibility for vehicle control to the vehicle. The potential failure of the steer-by-wire function must be handled immediately by redundancy concepts to prevent an unacceptable failure of the steering function. This places high demands on the mechatronic chassis systems to ensure functional and reliable vehicle control [2], [3].

The review of this article was arranged by Associate Editor Weichao Zhuang.

These requirements are met by providing hardware redundancy to components whose failure would result in a safety goal violation. According to Hales and Pattok [1], a system remains fully operational after a failure if a subsequent failure does not result in a safety goal violation. Otherwise, it remains operational but in an emergency mode and must be brought to a safe state. Redundancy can be achieved not only by using redundant hardware, but also by using cross-component functional redundancy, as in the architecture presented by Bergmiller [4].

An example of cross-actuator redundancy in the context of steer-by-wire is differential steering, also known as torque steer. Each driving and braking torque affects the steering system by generating a torque about the kingpin axis. If the two drive torques at the steered axle differ, their effect on the steering system is not balanced, and a steering torque remains. This steering torque can be controlled by determining the difference in drive torque between the two driven wheels while adjusting the sum of the drive torques to control the longitudinal motion [5], [6], [7], [8], [9], [10], [11], [12], [13], [14].

Differential steering has been studied in the literature for various purposes. In conventional steering systems, differential steering can replace electric power steering units and reduce the energy required for steering assistance [5], [6], [7]. The provision of redundancy in steer-by-wire systems based on differential steering is investigated on the one hand by using the brake system [8], [9] and on the other hand by using wheel-individual drives [10], [11], [12], [13] to control the steering angle. Other approaches omit the steering actuator by design and use a vehicle dynamics control approach to control both longitudinal and lateral motion with drive wheel torques only, such as the approaches proposed by Kuslits [14] for a front- and rear-axle steered vehicle and Seiffer et al. [15] for an articulated vehicle.

An overview of numerous control approaches for fault-tolerant vehicle motion control, including some approaches using differential steering, is given by Stolte [16].

A vehicle with multiple steering actuators or wheel-selective drives can be considered overactuated because there are more actuators than necessary to provide longitudinal and lateral guidance. On the one hand, overactuation can result from the need for redundancy. On the other hand, overactuation provides the opportunity to derive a certain allocation of actuator control variables that not only satisfies the primary control targets, but also considers further optimization objectives.

One way to resolve overactuation is to apply optimal control allocation approaches. These approaches are used, for example, to derive the control variables of a wheel-individual driven and/or steered vehicle. In addition to the realization of the specified vehicle motion, the optimization objectives can address the dynamic stability of the vehicle or the energy-optimal allocation of the control variables [17], [18].

Various studies have demonstrated the potential of using differential steering as a redundancy mechanism in steer-by-wire systems. These studies typically introduce holistic control approaches aimed at controlling the vehicle's trajectory, yaw rate, or steering angle through differential steering [10], [11], [12], [13], with most of the evidence based on simulation results. Some studies focus on assessing the vehicle control performance of the proposed strategies by comparing them to alternative control methods in scenarios where the steering actuator is initially failed from the beginning of the maneuver [10], [12], [13]. Others evaluate the control performance by comparing the proposed strategy without the use of the steering actuator against a reference strategy that is based on steering by using the steering actuator [8], [11].

However, an analysis of vehicle dynamics during the failure-induced transition from primary system operation to redundant system operation is not adequately addressed in the existing literature. From our perspective, ensuring a safe, stable, and imperceptible transition is a crucial factor when evaluating the suitability of cross-actuator redundancy.

To address this gap, we have developed an optimal control allocation approach that considers differential steering to allocate the drive and steering torques according to the current actuator state. This approach is employed both in a simulation study and in test drives using a demonstrator vehicle. The resulting measurements are used to analyze to what extent the vehicle can maintain its trajectory despite a sudden actuator failure, without compromising vehicle guidance—whether controlled by manual driver input or an automated driving system.

The contributions of our work are summarized as follows:

- We demonstrate that a control allocation approach downstream of the controller, which distributes the controller's torque outputs to the actuators, can provide both failure-free operation (with a functional steering actuator) and redundant operation via differential steering, without the need for controller reconfiguration. This makes the proposed approach universally applicable to other cascaded control structures.
- We provide a comprehensive analysis of vehicle dynamics behavior in the immediate aftermath of the actuator failure and the subsequent transition to differential steering control. This analysis includes a detailed evaluation of actuator torque, yaw rate, and lateral tracking error.
- Furthermore, we outline the feedback correction signals that must be provided to higher modules of the cascaded control structure to ensure seamless transitions between failure-free operation (via the steering actuator) and redundant operation (via differential steering).

This paper is organized as follows: Section II introduces the methodology of this work, including a description of the demonstrator vehicle, its vehicle guidance and dynamics controller, and an overview of the simulation model used. A summary of the fundamentals of differential steering functionality is then provided, followed by a description

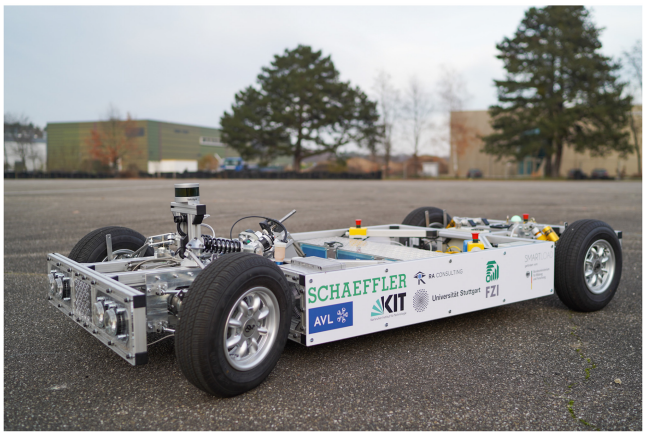

FIGURE 1. The demonstrator vehicle (scale 1:1.5) used for real-world validation tests. It is equipped with Ackermann steering, chassis kinematics optimized for differential steering [20] and wheel-selective drives on the front axle (two electric motors, each with 2.6 kW nominal power and 7.1 kW maximum power). Source: [22].

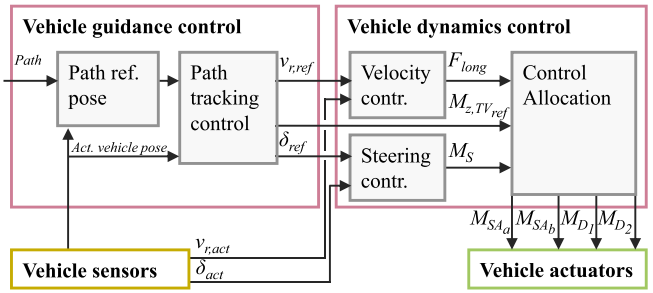

FIGURE 2. Control loop for lateral and longitudinal control of the demonstrator vehicle. The vehicle guidance controller outputs reference values for velocity at the rear axle $v_{r,ref}$, steering angle δ_{ref}, and torque vectoring torque $M_{z,TV_{ref}}$. Velocity and steering controller derive the overall driving force F_{long} and steering torque M_S which are allocated to the two driving motors (M_{D_1} and M_{D_2}) and the primary and redundant steering actuators (M_{SA_a} and M_{SA_b}). Adapted from [22].

of the proposed control allocation approach. The test and validation procedures, along with the maneuvers used for testing and validation, are subsequently presented. Section III presents a detailed analysis and discussion of the results from the simulation-based study and driving tests with the demonstrator vehicle. Finally, the conclusion and outlook are provided in Section IV.

II. METHODS AND PROCEDURES

A. DEMONSTRATOR VEHICLE AND SIMULATION MODEL

A 1:1.5 scale demonstrator vehicle (Fig. 1) and its simulation model were used to develop, simulate, and validate the proposed approach, as well as to investigate the vehicle guidance behavior in the event of actuator failures. The vehicle has two steering actuators (primary and redundant) and wheel-selective drives on the steered front axle (Ackermann steering), so that both a classical hardware redundancy concept and cross-actuator functional redundancy for the steering function can be implemented. The vehicle was originally developed in the context of the E^2-LENK project [19] and used by Römer [5] and Kautzmann [20] in their dissertations focusing on steering assistance by means of wheel-selective drive control. Modifications to the vehicle were made as part of the SMARTLOAD project, including the addition of automated driving capability and differential steering control to provide functional redundancy for the steering actuator [21]. The vehicle's control structure and simulation model are described in more detail below. An overview of the specifications of the demonstrator vehicle is given in Appendix A.

1) LATERAL AND LONGITUDINAL VEHICLE CONTROL

The vehicle control loop is a cascaded control approach (see Fig. 2). Several modes of operation are available.

For longitudinal control, the input variable can be the total driving force F_{long} or the velocity at the rear axle $v_{r,ref}$, which is converted to a corresponding driving force F_{long} by the velocity controller. Steering is accomplished by the steering controller, which calculates the total steering torque M_S based on the steering angle reference input δ_{ref}.

In the default setup, the control allocation module splits the total drive force F_{long} equally between the two wheels and uses one of the steering actuators for steering. An implementation of this controller configuration can be accessed via [23].

The vehicle guidance controller module adds automated driving capability to the approach. A path with a velocity profile can be defined offline and serves as static input to the path tracking controller, which defines the reference velocity $v_{r,ref}$ and steering angle δ_{ref}. The control approach is an extended version of the Stanley controller that compensates for system delay to improve tracking accuracy [22]. For the investigation within this work, we slightly modified the path tracking controller to additionally output the torque vectoring torque $M_{z,TV_{ref}}$, as described in Appendix B.

Accurate localization data for automated driving functionality is provided by a multi-sensor RTK-GNSS device that uses Real-Time Kinematic (RTK) positioning based on Global Navigation Satellite System (GNSS) signals.

The control algorithms are implemented in MATLAB SIMULINK and run on a DSPACE MICROAUTOBOX control unit. Refer to [22] for more information on the control approaches described above, including the MATLAB SIMULINK implementation of both vehicle guidance and vehicle dynamics control.

2) SIMULATION MODEL

For the simulation studies, an existing model of the demonstrator vehicle was utilized, implemented in the vehicle simulation environment IPG CARMAKER 8.0. This model runs in co-simulation with MATLAB SIMULINK, utilizing the CARMAKER extension CARMAKER FOR SIMULINK [24].

The vehicle's kinematics and driving dynamics are represented by corresponding CARMAKER project files, while selected subsystems are modeled in MATLAB SIMULINK to address vehicle-specific real-world imperfections, such as

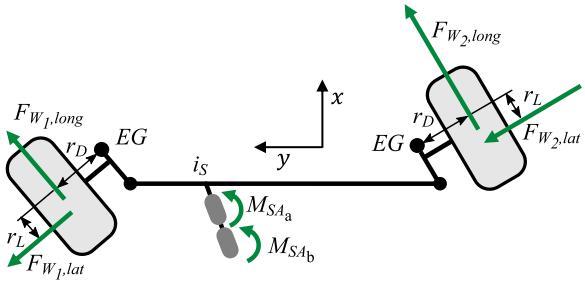

FIGURE 3. Planar representation of the chassis kinematics of the demonstrator vehicle with the relevant forces and torques that influence the steering motion (rotation of the wheels around their steering axis *EG*). The lateral forces of the tires ($F_{W_1,lat}$ and $F_{W_2,lat}$) affect the steering torque via the lateral force arm (r_L), the driving forces ($F_{W_1,long}$, $F_{W_2,long}$) via the interfering force arm r_D, and the torques of the primary and redundant steering actuators (M_{SA_a}, M_{SA_b}) via the steering ratio i_S (gear ratio between the steering axis *EG* and the actuator shaft). Adapted from [5], [25].

signal rates and steering delays. In particular, the actuator dynamics, as well as the elasticity and friction effects of the steering system, were modelled on a more detailed level. Furthermore, the vehicle guidance, dynamics, steering, and speed controllers, along with the control allocation functionality, are also implemented in MATLAB SIMULINK. As MATLAB SIMULINK was utilized throughout the development toolchain for both simulation and the vehicle's ECU, the implementation could be directly transferred to the real vehicle.

The simulation model of the demonstrator vehicle is available at [23] including a more detailed description of the modelling.

B. DIFFERENTIAL STEERING

The functional principle of differential steering as cross-actuator functional redundancy for the steering actuation is shown in Fig. 3. The chassis kinematics are simplified as a planar projection (which corresponds to suspension kinematics with a kingpin inclination angle and a caster angle of 0°). This makes it easier to understand the effects of the forces and torques shown. The derivation follows the approach of Römer [5]. In his dissertation he describes the effect of differential steering to reduce the steering torque at the steering wheel, thus replacing the functionality of an electric power steering actuator.

In contrast, we consider a steer-by-wire vehicle without a mechanical connection to the steering wheel or an automated vehicle in the following. However, the basic effect of differential steering remains the same.

As Römer [5] we first assume a static scenario and neglect the forces of inertia, elasticity, and damping. The equilibrium of forces and torques with respect to the steering axis *EG* according to Fig. 3 is given by

$$\begin{aligned} 0 = &-\Delta F_{W_{1,2},long} r_D + F_{W_{1,2},lat} r_L \\ &- \left(M_{SA_a} + M_{SA_b}\right) i_S \end{aligned} \tag{1}$$

with the lateral force of the front axle

$$F_{W_{1,2},lat} = F_{W_1,lat} + F_{W_2,lat} \tag{2}$$

and the torque vectoring force

$$\Delta F_{W_{1,2},long} = F_{W_2,long} - F_{W_1,long}. \tag{3}$$

The vehicle controller can directly influence the primary and redundant steering actuator torques, M_{SA_a} and M_{SA_b}, as well as the drive forces, $F_{W_1,long}$ and $F_{W_2,long}$, which result from the drive motor torques, M_{D_1} and M_{D_2}. However, the tire lateral forces, $F_{W_1,lat}$ and $F_{W_2,lat}$, are a result of vehicle dynamics and effects in the wheel-road contact area.

Since unequal driving forces $F_{W_1,long}$ and $F_{W_2,long}$ cause the torque vectoring yaw torque $M_{z,TV}$, they also change the lateral force distribution between the front and rear axles, as derived by Römer [5]. For the influence of the torque vectoring force $\Delta F_{W_{1,2},long}$ on the lateral forces of the front axle $F_{W_{1,2},lat}$ and rear axle $F_{W_{3,4},lat}$ he finds

$$\begin{aligned} \Delta F_{W_{1,2},lat} &= -\frac{1}{l\cos(\delta_{act})} M_{z,TV} \\ &= -\frac{w}{2l} \Delta F_{W_{1,2},long}, \\ \Delta F_{W_{3,4},lat} &= \frac{1}{l} M_{z,TV} = \frac{w}{2l} \cos(\delta_{act}) \Delta F_{W_{1,2},long} \end{aligned} \tag{4}$$

with the wheelbase l, track width w and actual steering angle δ_{act}. We define $F^*_{W_{1,2},lat}$ as the lateral force on the front axle for the case of $\Delta F_{W_{1,2},long} = 0\,\mathrm{N}$ and we get

$$F_{W_{1,2},lat} = F^*_{W_{1,2},lat} - \frac{\Delta F_{W_{1,2},long} w}{2l}. \tag{5}$$

We rearrange (1) taking into account (5), cluster the actuator-dependent ($M_{S,Ctrl}$) and external ($M_{S,ext}$) quantities, and add M_{dis} to account for any neglected effects that affect the steering system dynamics. This results in

$$\begin{aligned} &\underbrace{\left(M_{SA_a} + M_{SA_b}\right) i_S + \Delta F_{W_{1,2},long} \left(r_D + \frac{r_L w}{2l}\right)}_{M_{S,Ctrl}} \\ &= \underbrace{F^*_{W_{1,2},lat} r_L + M_{dis}}_{M_{S,ext}}. \end{aligned} \tag{6}$$

When designing the suspension, an optimization of the lateral force arm r_L and the interfering force arm r_D can be performed with respect to the differential steering functionality, taking into account other optimization objectives of the chassis design process [20], [26].

C. CONTROL ALLOCATION APPROACH

The task of the proposed control allocation approach is to specify the steering actuator and drive torques such that the control objectives are optimally achieved while satisfying the current constraints on the actuator and drive torques. This is accomplished by solving a constrained weighted least squares problem resolving the overactuation by minimizing a cost function under the given constraints [27]. Fig. 4 illustrates the proposed control allocation approach.

The input variables (control objectives) are the total front axle drive force F_{long}, the total steering torque M_S referred to the steering axis *EG*, and the torque vectoring torque $M_{z,TV_{ref}}$.

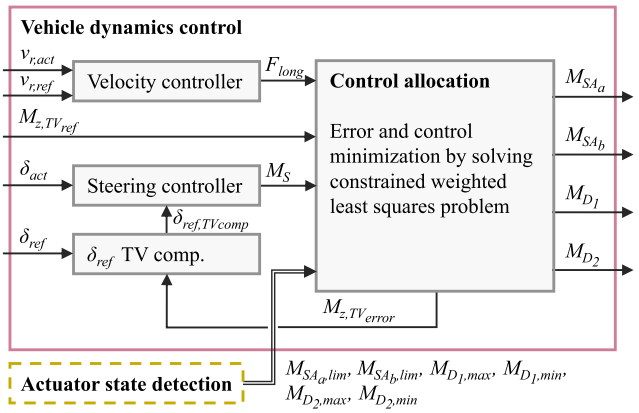

FIGURE 4. Proposed control architecture with constrained control allocation to redistribute the actuator torques with respect to the current actuator constraints. The effect of unintended torque vectoring caused by the redistribution is compensated by an offset on the δ_{ref} input. Adapted from [15].

The torque vectoring torque $M_{z,TV_{ref}}$ is the additional yaw torque caused by drive force difference at the front axle. It is an optional input that can originate from an extended path tracking controller or a vehicle stability controller.

The output variables (actual controls) are the four actuator or motor torques M_{SA_a}, M_{SA_b}, M_{D_1}, and M_{D_2}.

Differential steering functionality is obtained by considering the effect of different drive torques on the steering torque in the control effectiveness matrix which is part of the cost function. Thus, the effect is taken into account when specifying the actual controls.

The current limits of the actuator torques are specified by the actuator state detection module and include the torque limits of the steering actuators $M_{SA_a,lim}$ and $M_{SA_b,lim}$ as well as the maximum and minimum drive torques $M_{D_1,max}$, $M_{D_1,min}$, $M_{D_2,max}$, and $M_{D_2,min}$.

The limits result from technical data of the actuators, e.g., torque-speed characteristics, from diagnosis data of the actuator control unit, e.g., temperature-related derating, or from sensor-based vehicle diagnosis systems that can detect limitations or failures, as evaluated, e.g., by Li et al. [28].

In the failure-free case, the actual controls are specified based on the defined weights of the cost function. The weights can be adjusted dynamically, e.g., to balance the load between the actuators and provide thermal protection to prevent overheating.

In the case of a total failure of, e.g., a steering actuator, its constraint is set to 0 Nm. By taking the constraint into account when solving the optimization problem, an alternative combination of actual controls is immediately output that correctly realizes the control objectives [15]. Thus, the error does not affect the upstream control loops, since their output variables are correctly exploited.

Differential steering not only affects the steering torque, but also induces an additional yaw torque that affects the yaw rate (torque vectoring) [5]. Without taking this effect into account, compensating for a steering actuator failure with differential steering would result in an unaffected realization of the desired steering angle δ_{ref}. However, the resulting yaw rate, and thus the vehicle motion, would differ from its state prior to actuator failure. To keep the vehicle's behavior consistent despite the failure, the unintended torque vectoring effect on the yaw rate must be compensated. We accomplished this by adjusting the δ_{ref} input to the steering controller accordingly.

In the following, we describe the chosen constraint control allocation algorithm and derive the control effectiveness and weighting matrices as well as the equations for the torque vectoring compensation functionality.

1) CONSTRAINT CONTROL ALLOCATION ALGORITHM

The control allocation problem according to Oppenheimer et al. [27] is to find the control vector $\boldsymbol{\delta}$ such that

$$\boldsymbol{B}\boldsymbol{\delta} = \boldsymbol{d}_{des} \tag{7}$$

and

$$\underline{\boldsymbol{\delta}} < \boldsymbol{\delta} \leq \overline{\boldsymbol{\delta}} \tag{8}$$

with the control effectiveness matrix $\boldsymbol{B}$, the control objective vector $\boldsymbol{d}_{des}$ and the lower and upper constraints of the actual controls $\underline{\boldsymbol{\delta}}$ and $\overline{\boldsymbol{\delta}}$.

In order to solve (7), we formulate the control allocation problem as a mixed optimization problem, as described by Oppenheimer et al. [27] and Härkegård [29]. Its objective is to determine $\boldsymbol{\delta}$ in such a way that it minimizes the cost function

$$J = \|\boldsymbol{W}_{\delta}(\boldsymbol{\delta} - \boldsymbol{\delta}_p)\|^2 + \gamma \|\boldsymbol{W}_{d_{des}}(\boldsymbol{B}\boldsymbol{\delta} - \boldsymbol{d}_{des})\|^2 \tag{9}$$

with the 2-norm $\|\boldsymbol{u}\|^2 = \boldsymbol{u}^T\boldsymbol{u}$, the diagonal weighting matrices $\boldsymbol{W}_{\delta}$ and $\boldsymbol{W}_{d_{des}}$ and the preferred control vector $\boldsymbol{\delta}_p$.

In order to prioritize the minimization of the control error over that of the control vector, a high value of the weighting factor γ should be selected [29]. In the following, we set $\gamma = 1$ and instead achieve a higher relative weighting of the second term compared to the first term in (9) by assigning larger values to the elements of the weighting matrix $\boldsymbol{W}_{d_{des}}$ than to those of the weighting matrix $\boldsymbol{W}_{\delta}$ [15].

With

$$\boldsymbol{\delta}_p = \begin{bmatrix} 0 & 0 & 0 & 0 \end{bmatrix}^T \tag{10}$$

the optimal control vector $\boldsymbol{\delta}_{opt}$ is obtained by

$$\boldsymbol{\delta}_{opt} = \arg \min_{\underline{\boldsymbol{\delta}} < \boldsymbol{\delta} \leq \overline{\boldsymbol{\delta}}} \|\boldsymbol{W}_{\delta}\boldsymbol{\delta}\|^2 + \|\boldsymbol{W}_{d_{des}}(\boldsymbol{B}\boldsymbol{\delta} - \boldsymbol{d}_{des})\|^2 \tag{11}$$

For solving (11) we chose the active-set algorithm provided by the *quadprog* function in MATLAB [30]. Active-set algorithms are recommended by Härkegård [29] because they converge to a feasible solution even if more than one actual control reaches its constraint during the solving iterations, which is not always the case with other algorithms.

The *quadprog* function uses the following notation for the cost function [30].

$$\boldsymbol{x}_{opt} = \arg\min_{\boldsymbol{lb} \leq \boldsymbol{x} \leq \boldsymbol{ub}} \frac{1}{2}\boldsymbol{x}^T\boldsymbol{H}\boldsymbol{x} + \boldsymbol{c}^T\boldsymbol{x} \tag{12}$$

To make this notation consistent with (11) we first resolve the 2-norm functions and get

$$\begin{aligned}\boldsymbol{\delta}_{opt} = \arg\min_{\underline{\boldsymbol{\delta}} < \boldsymbol{\delta} \leq \overline{\boldsymbol{\delta}}} \Big(& \boldsymbol{\delta}^T \boldsymbol{W}_{\delta}^* \boldsymbol{\delta} \\ & + (\boldsymbol{B}\boldsymbol{\delta} - \boldsymbol{d}_{des})^T \boldsymbol{W}_{d_{des}}^* (\boldsymbol{B}\boldsymbol{\delta} - \boldsymbol{d}_{des}) \Big)\end{aligned} \tag{13}$$

with

$$\begin{aligned}\boldsymbol{W}_{\delta}^* &= \boldsymbol{W}_{\delta}^T \boldsymbol{W}_{\delta} \\ \boldsymbol{W}_{d_{des}}^* &= \boldsymbol{W}_{d_{des}}^T \boldsymbol{W}_{d_{des}}.\end{aligned} \tag{14}$$

In order to match (11) with (12) we finally find

$$\begin{aligned}\boldsymbol{x} &= \boldsymbol{\delta} \\ \boldsymbol{H} &= \boldsymbol{B}^T \boldsymbol{W}_{d_{des}}^* \boldsymbol{B} + \boldsymbol{W}_{\delta}^* \\ \boldsymbol{c} &= -\boldsymbol{B}^T \boldsymbol{W}_{d_{des}}^* \boldsymbol{d}_{des} \\ \boldsymbol{lb} &= \underline{\boldsymbol{\delta}} \\ \boldsymbol{ub} &= \overline{\boldsymbol{\delta}}.\end{aligned} \tag{15}$$

2) CONTROL EFFECTIVENESS AND WEIGHTING MATRICES

According to (7) and Fig. 4 we define the control objective vector $\boldsymbol{d}_{des}$ and the control vector $\boldsymbol{\delta}$ as

$$\boldsymbol{d}_{des} = \begin{bmatrix} M_S & F_{long} & M_{z,TV_{ref}} \end{bmatrix}^T \tag{16}$$

and

$$\boldsymbol{\delta} = \begin{bmatrix} M_{SA_a} & M_{SA_b} & M_{D_1} & M_{D_2} \end{bmatrix}^T. \tag{17}$$

The lower and upper constraints of the actual controls $\underline{\boldsymbol{\delta}}$ and $\overline{\boldsymbol{\delta}}$ are given by

$$\begin{aligned}\underline{\boldsymbol{\delta}} &= \begin{bmatrix} -M_{SA_a,lim} & -M_{SA_b,lim} & M_{D_1,min} & M_{D_2,min} \end{bmatrix}^T \\ \overline{\boldsymbol{\delta}} &= \begin{bmatrix} M_{SA_a,lim} & M_{SA_b,lim} & M_{D_1,max} & M_{D_2,max} \end{bmatrix}^T.\end{aligned} \tag{18}$$

The overall steering torque M_S results from the actuator-dependent quantities $M_{S,Ctrl}$ in (6). With (3), the dynamic wheel radius r_W, and drive motor gear ratio i_{DG} we get

$$\Delta F_{W_{1,2},long} = \left(M_{D_2} - M_{D_1}\right)\frac{i_{DG}}{r_W}. \tag{19}$$

Inserting (19) in (6) finally yields

$$M_S = i_S M_{SA_a} + i_S M_{SA_b} - b_{DS} M_{D_1} + b_{DS} M_{D_2} \tag{20}$$

with

$$b_{DS} = \frac{i_{DG}}{r_W}\left(r_D + \frac{r_L w}{2l}\right). \tag{21}$$

The overall drive torque F_{long} and the torque vectoring reference $M_{z,TV_{ref}}$ are obtained by

$$F_{long} = \frac{i_{DG}}{r_W} M_{D_1} + \frac{i_{DG}}{r_W} M_{D_2} \tag{22}$$

and

$$M_{z,TV_{ref}} = -b_{TV} M_{D_1} + b_{TV} M_{D_2}. \tag{23}$$

Taking into account (4) and (19) b_{TV} becomes

$$b_{TV} = \frac{i_{DG} w}{2 r_W} \cos(\delta_{act}). \tag{24}$$

With (20), (22) and (23) the control effectiveness matrix $\boldsymbol{B}$ becomes

$$\boldsymbol{B} = \begin{bmatrix} i_S & i_S & -b_{DS} & b_{DS} \\ 0 & 0 & \frac{i_{DG}}{r_W} & \frac{i_{DG}}{r_W} \\ 0 & 0 & -b_{TV} & b_{TV} \end{bmatrix}. \tag{25}$$

The behavior of the control allocation is defined by the parameters of the diagonal weighting matrices $\boldsymbol{W}_{\delta}^*$ and $\boldsymbol{W}_{d_{des}}^*$. A weighting factor is assigned to each of the control objectives and actual controls.

$$\begin{aligned}\boldsymbol{W}_{\delta}^* &= diag\left(W_{SA_a}, W_{SA_b}, W_{D_1}, W_{D_2}\right) \\ \boldsymbol{W}_{d_{des}}^* &= diag\left(W_S, W_{long}, W_{z,TV}\right)\end{aligned} \tag{26}$$

The control allocation approach used is based on a weighted least squares problem that combines both control and error minimization. When choosing the weighting factors, it is therefore important that minimizing the errors $(\boldsymbol{B}\boldsymbol{\delta} - \boldsymbol{d}_{des})$ has a higher priority than minimizing the controls $\boldsymbol{\delta}$ [29]. This priority of weighting factors yields the desired distribution of actual controls if the control objectives can be fully met by the corresponding actual controls without reaching their constraints.

However, if one of the actual controls is constrained in such a way that not all of the control objectives can be met, prioritization of the control objectives is required. The way this is done in a specific application depends heavily on the use cases of the vehicle, such as maximum velocity or operating area (public road or non-public fenced area), the configuration and specification of the components (e.g., one or two steering actuators, additional mechanical friction brake for braking), and the resulting fail-safe concept of the vehicle. A situation-dependent prioritization is also conceivable (e.g., lower weighting of the drive force control objective during acceleration than during braking). For the demonstrator vehicle and the tests conducted within this work, we determined that meeting the steering torque target has the highest priority, followed by meeting the drive force target. In contrast, meeting the torque vectoring objective has a low priority.

For the weighting of a control objective or an actual control within the cost function, not only the relative amount of the respective weighting factor is decisive, but also the absolute size of the value range of the corresponding control variable (see Table 5 in Appendix A). For example, the range for M_{SA_a} and M_{SA_b} is from $-0.45\,\text{Nm}$ to $0.45\,\text{Nm}$, while F_{long} can assume values from $-2004\,\text{N}$ to $2004\,\text{N}$. If the weighting factors of both quantities are of similar magnitude, the required prioritization of error minimization over control minimization is still given.

Finally, the following values of the weighting factors for the experiments within the scope of this study result from the above considerations: $W_{SA_a} = 10^1$, $W_{SA_b} = 10^1$, $W_{D_1} = 10^0$, $W_{D_2} = 10^0$, $W_S = 10^7$, $W_{long} = 10^3$, $W_{z,TV} = 10^1$.

3) TORQUE VECTORING COMPENSATION

As in Römer [5], we consider the linear bicycle model to derive the effect of differential steering on the yaw rate and how the steering angle reference needs to be adjusted to compensate for this effect.

For small steering angles δ and small vehicle sideslip angles β this yields

$$\begin{aligned}\alpha_{1,2} &= \delta - \beta - a\frac{\dot{\psi}_{act}}{v_{act}}\\ \alpha_{3,4} &= -\beta + b\frac{\dot{\psi}_{act}}{v_{act}}\end{aligned} \tag{27}$$

with the tire slip angles for the front wheel $\alpha_{1,2}$ and the rear wheel $\alpha_{3,4}$, the velocity v_{act}, yaw rate $\dot{\psi}_{act}$, distance of the center of gravity to the front axle a, and distance of the center of gravity to the rear axle b.

The tire characteristics are defined by the cornering stiffness of the tire pairs on the front axle $C_{y_{1,2}}$ and the rear axle $C_{y_{3,4}}$. The lateral forces of the two axles ($F_{W_{1,2},lat}$, $F_{W_{3,4},lat}$) are given by

$$\begin{aligned}F_{W_{1,2},lat} &= C_{y_{1,2}}\alpha_{1,2}\\ F_{W_{3,4},lat} &= C_{y_{3,4}}\alpha_{3,4}.\end{aligned} \tag{28}$$

We define $\Delta\delta_{ref}$ to be the steering angle adjustment which needs to be applied so that the lateral force changes $\Delta F_{W_{1,2},lat}$ and $\Delta F_{W_{3,4},lat}$ (see (4)) caused by differential steering remain without affecting the yaw rate $\dot{\psi}_{act}$. Therefore, we require that $\dot{\psi}_{act}$ remains constant. Thus, we omit $\Delta\dot{\psi}_{act}$, and obtain from (27) and (28)

$$\begin{aligned}\Delta F_{W_{1,2},lat} &= C_{y_{1,2}}\left(\Delta\delta_{ref} - \Delta\beta\right)\\ \Delta F_{W_{3,4},lat} &= -C_{y_{3,4}}\Delta\beta.\end{aligned} \tag{29}$$

By replacing $\Delta F_{W_{1,2},lat}$ and $\Delta F_{W_{3,4},lat}$ with the expressions in (4) and resolving to $\Delta\delta_{ref}$, we get

$$\Delta\delta_{ref} = -\Delta F_{W_{1,2},long}\frac{w}{2l}\left(\frac{1}{C_{y_{1,2}}} + \frac{\cos(\delta_{act})}{C_{y_{3,4}}}\right). \tag{30}$$

The adjusted reference steering angle $\delta_{ref,TVcomp}$ is a function of the torque vectoring torque to be compensated, $M_{z,TV_{error}}$. It is given by (19), (23), and (30) as

$$\delta_{ref,TVcomp} = \delta_{ref} - k_{\delta,M_z}M_{z,TV_{error}} \tag{31}$$

with

$$k_{\delta,M_z} = \frac{1}{l}\left(\frac{1}{C_{y_{1,2}}\cos(\delta_{act})} + \frac{1}{C_{y_{3,4}}}\right). \tag{32}$$

The torque vectoring error $M_{z,TV_{error}}$ contains only the part of the torque vectoring torque that is applied by the control allocation for the purpose of differential steering. Otherwise the effect of the intended torque vectoring reference $M_{z,TV_{ref}}$ would also be compensated. To calculate it we solve the control allocation problem (7) with the modified control objective vector $\boldsymbol{d}^*_{des} = \begin{bmatrix}M_S & F_{long} & 0\end{bmatrix}^T$. The control vector $\boldsymbol{\delta}^*$ includes the drive torques $M^*_{D_1}$ and $M^*_{D_2}$ that would result if the torque vectoring reference $M_{z,TV_{ref}}$ was neglected. $M_{z,TV_{error}}$ is obtained by considering (23) resulting in

$$M_{z,TV_{error}} = -b_{TV}M^*_{D_1} + b_{TV}M^*_{D_2}. \tag{33}$$

4) IMPLEMENTATION

The described approach was implemented in MATLAB SIMULINK according to the architecture shown in Figure 4. The modules were integrated into the vehicle simulation model, which is published in [23], together with the path tracking controller from [22] and its adaptations described in the Appendix B.

The input signal rate (sensor data) and the output rate of the actuator torque targets were limited to 100 Hz to match the actual signal rates of the real vehicle. The path tracking controller's frequency was set to 100 Hz. Since the $M_{z,TV_{error}}$ signal is fed back to the torque vectoring compensation module, an inner cascade loop is obtained that also includes the steering controller and control allocation modules. These modules have been set to a frequency of 1000 Hz to ensure a higher frequency for the inner loop of the cascaded system compared to the outer loop.

To prevent an algebraic loop, the $M_{z,TV_{error}}$ signal was delayed by 1 ms. In addition, a 1 ms delay in the control allocation input signals of the actuator constraints $\underline{\boldsymbol{\delta}}$ and $\overline{\boldsymbol{\delta}}$ was found to provide a smooth transition during abrupt constraint changes in the event of a failure.

Furthermore, the anti-windup in the velocity and steering angle controllers was adjusted to dynamically set the maximum controller output based on the current system performance derived from the actuator state. To ensure the approach's applicability to the demonstrator vehicle under real-world disturbances and noisy sensor signals, filters were applied to various signals.

D. TEST AND VALIDATION PROCEDURE

To test and validate the proposed approach and to investigate the vehicle guidance behavior in the event of actuator failures, two driving maneuvers, steady-state circular driving and the double lane change maneuver, were used. The steady-state circular driving allows the investigation of actuator failures in a steady-state vehicle dynamic condition. The objective was to ensure that the vehicle motion, i.e., velocity and yaw rate, continued unaffected and that there was no deviation from the driven circular path. This maneuver was executed with constant steering angle input and also with path input, representing both manual and automated driving scenarios.

In contrast, the double lane change is a transient driving maneuver in which the dynamics change significantly. The vehicle must be able to perform the maneuver without

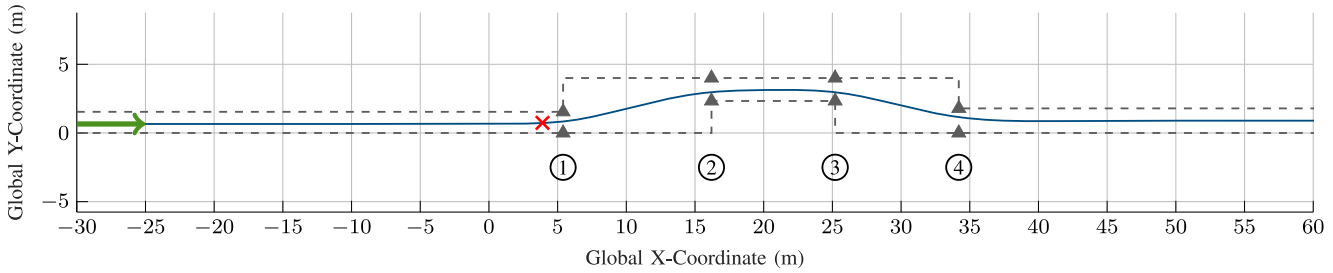

FIGURE 5. Map of the double lane change maneuver based on the ISO 3888-1 standard [32], modified according to the vehicle scale and the reduced velocity of 8 m/s. The four pairs of cones mark the corners of the gray dashed lines representing the lane boundaries. Their coordinates for the two velocities considered are given in Table 2. The blue line is the reference path used as input for the path tracking controller. The vehicle's starting point is indicated by the green arrow. The red cross indicates the point at which actuator failures are initiated since it was found to be the position with the highest required steering torque.

exceeding the lane boundaries, even if an actuator fails during a highly dynamic driving situation.

In the following, the vehicle configuration, maneuvers, and failure scenarios are considered in more detail.

1) REDUNDANCY CONFIGURATION AND LIMITATION OF THE ACTUATORS

The vehicle equipped with two steering actuators and individual wheel drives allows for different redundancy configurations. Since our research focus is on cross-actuator functional redundancy concepts, we chose a single steering actuator configuration with differential steering as the redundancy.

In addition to the constraints imposed by actuator failure, other constraints result from the torque-speed characteristics of the actuator. The motors of the demonstrator vehicle provide sufficient wheel torque to reach the longitudinal slip limit up to a velocity of 5.5 m/s. As the velocity increases, the maximum torque decreases and so does the differential steering capability.

As this limitation is due to the selection of components and not a limitation of the proposed approach, we took the following measures to eliminate this limitation in our investigations. For the demonstrator vehicle test, we limited the velocity to 5.5 m/s, and for the simulation study, we virtually increase the ability of the drives to maintain sufficient torque up to the maximum vehicle velocity of 8 m/s. Therefore, more dynamic driving situations could be considered in the simulation study.

2) DRIVING MANEUVERS AND FAILURE SCENARIOS

The steady-state circular driving maneuver starts with a straight-line acceleration phase until the constant target velocity $v_{r,ref}$ is reached, followed by a step-steer leading to a circular motion. The vehicle can execute the maneuver either by using the path tracking controller, which keeps the vehicle's reference point (center of the rear axle) on the defined circle with constant radius $R_{r,ref}$, or in an open loop mode by specifying a constant target steering angle δ_{ref}.

The combination of velocity and radius or steering angle determines the lateral acceleration a_y and yaw rate $\dot{\psi}$ of the maneuver and thus the dynamic state of the vehicle.

TABLE 1. Specification of the steady-state circular driving maneuver.

$v_{r,ref}$	$R_{r,ref}$	δ_{ref}	a_y	$\dot{\psi}$
8.0 m/s	24.0 m	0.089 rad	2.67 m/s^2	0.33 rad/s

We have based the specification of the maneuvers on the recommendation of the ISO 7401 standard [31] for step-steer maneuvers, which requires a minimum lateral acceleration of 4.00 m/s^2. Considering the 1:1.5 scale of the vehicle, the minimum lateral acceleration is 2.67 m/s^2.

Table 1 summarizes the resulting specification for the steady-state circular driving maneuver.

The double lane change maneuver is defined by the limits of the lanes that the vehicle must comply with. We derived the positions of the boundary cones from the ISO 3888-1 standard [32]. It describes the maneuver for a velocity of 80 km/h (22.22 m/s). To make the maneuver comparably challenging for lower speeds and the 1:1.5 scale vehicle, we have made the following adjustments to the positions of the cones. The x-coordinates of the cones have been reduced by the factor of the reduced velocity compared to the standard velocity, so that the duration of the lane change remains comparable. The y-coordinates of the boundaries, and thus the width of the lane and the width of the obstacle to be avoided by the vehicle, have been reduced by the factor of the vehicle scale.

The resulting boundaries for the lane change maneuver at 8 m/s are shown in Fig. 5. The positions of the boundary cones for 8 m/s and 5.5 m/s are given in Table 2. The target path, which defines the movement of the vehicle with respect to the center of the rear axle, was generated by spline interpolation and transformed into the format appropriate for the path tracking controller (see [22]). The velocity profile defines the acceleration before entering the lane change section, and according to the ISO 3888-1 standard [32], once the target velocity is reached, the drive force F_{long} is kept constant without compensating for velocity deviations.

We considered different failure scenarios based on the two maneuvers. One of the failure scenarios is the permanent failure of the steering actuator. Since the drive motors affect the steering torque, we also needed to investigate how the permanent failure of the right or left drive affects the steering

TABLE 2. Positions of the four pairs of cones marking the left and right lane boundaries of the double lane change maneuver (see Fig. 5). X-coordinates $x_{v_{8.0}}$ and $x_{v_{5.5}}$ differ depending on the vehicle velocity (8 m/s in simulation and 5.5 m/s for the demonstrator vehicle test drives).

Cone pair	$x_{v_{8.0}}$	$x_{v_{5.5}}$	y_{left}	y_{right}
#1	5.40 m	3.71 m	1.54 m	0.00 m
#2	16.20 m	11.14 m	4.00 m	2.33 m
#3	25.20 m	17.33 m	4.00 m	2.33 m
#4	34.20 m	23.51 m	1.79 m	0.00 m

capability and how it is compensated by the approach. Both in the simulation and on the demonstrator vehicle ECU, the failures were emulated by overwriting the corresponding torque setpoint with 0 Nm.

For the circular driving maneuver, the failure was injected after reaching a steady state driving dynamic condition. For the lane change maneuver, the focus was on considering a worst case scenario. Therefore, the turn-in point when passing the pair of cones #1 (see Fig. 5) was chosen as the failure injection point, since this point was found to have the highest steering torque requirements.

III. RESULTS AND DISCUSSION

The experimental plan for both the simulation study and the demonstrator vehicle test drives is presented first. Next, the plots prepared and the metrics calculated for analysis are described. The results of the simulation test drives are then presented and discussed in detail. Finally, the findings are validated by presenting the results of the test drives conducted with the demonstrator vehicle.

A. EXPERIMENTAL PLAN

The experimental plan for the simulation and demonstrator vehicle experiments included the driving maneuvers and failure scenarios considered in Section II-D2. Moreover, the control allocation settings were modified to examine the impact of omitting the torque vectoring compensation function.

The experiments that have been carried out for this work are shown in Table 3. Each experiment is assigned an ID which indicates the type of experiment (simulation "S" or demonstration vehicle "D"), the maneuver (circle with constant steering angle "C_δ", circle with constant radius "C_r" and double lane change "LC") and the failure scenario (steering actuator "fS", drive motor left "fD1" drive motor right "fD2") and the deviation from the default control allocation setup (without TV compensation "noComp").

To account for the redundancy configuration under consideration, the redundant steering actuator was permanently disabled in all experiments by choosing $M_{SA_b} = 0\,\text{Nm}$ in the constraint vectors.

B. PLOTS AND METRICS

To evaluate the experiments, plots were created and metrics were calculated. The data shown in the plots are the actual actuator and motor torques ($M_{SA_a,act}$, $M_{D_1,act}$ and $M_{D_2,act}$), the reference steering angle δ_{ref}, the adjusted reference steering angle $\delta_{ref,TVcomp}$ and the actual steering angle δ_{act} as well as the resulting yaw rate $\dot{\psi}_{act}$ and additionally the crosstrack error $e_{lat,r}$ for the maneuvers driven by the path tracking controller.

Metrics were applied to relevant intervals of the maneuver to quantitatively compare the different setups and failure scenarios to the failure-free test drive. For the steady-state circular maneuver, an evaluation interval of 4 s after the failure was chosen. On this interval the maximum and root-mean-square (RMS) steering angle control error ($\delta_{error,max}$ and $\delta_{error,RMS}$), the maximum and RMS deviation of the yaw rate from the value before the failure ($\Delta\dot{\psi}_{max}$ and $\Delta\dot{\psi}_{RMS}$), and the maximum and RMS deviation of the crosstrack error from the value before the failure ($\Delta e_{lat,r_{max}}$ and $\Delta e_{lat,r_{RMS}}$) were calculated.

For the double lane change maneuvers, the metric evaluation was applied to the path section with x-coordinates between 0 m and 40 m (vehicle velocity 8 m/s) and 0 m and 27.5 m (vehicle velocity 5.5 m/s), respectively. As for the circular maneuver, the maximum and RMS steering angle control error ($\delta_{error,max}$ and $\delta_{error,RMS}$) were calculated. The other metrics are the maximum and RMS crosstrack error ($e_{lat,r_{max}}$ and $e_{lat,r_{RMS}}$) and the minimum distance of the vehicle to the lane boundaries ($d_{lim,min}$).

The resulting metrics are summarized in Table 4.

C. SIMULATION VEHICLE TEST DRIVE RESULTS

1) STEADY-STATE CIRCULAR DRIVING

In the first experiment (S01), the basic functionality of the proposed control allocation approach was investigated. The sudden failure of the steering actuator was to be maintained by differential steering while keeping the steering angle constant during the circular driving maneuver. The first line of plots in Fig. 6 shows the simulation results.

After the failure, the differential drive torque is immediately adjusted, resulting in a right motor torque of 10 Nm and a left motor torque of −5 Nm, effectively satisfying both the total drive torque and differential steering torque requirements. As a result of the failure, the steering angle deviates slightly by 0.0011 rad (equivalent to 1.2% of the steering angle setpoint), but returns to its original value within 0.08 s. In response to this deviation, the differential drive torque temporarily increases after the failure before stabilizing at a constant level.

These results clearly demonstrate the effectiveness of the cascade approach, where the control allocation immediately redistributes the drive torques, eliminating the need for a significant response from the steering angle controller. It can also be concluded that the established control effectiveness matrix $\boldsymbol{B}$ and the included equation for the differential steering factor b_{DS} are valid.

The yaw rate increases as expected due to torque vectoring, changing by 23% from 0.338 rad/s to 0.416 rad/s, including a brief peak that coincides with the peak in the differential drive torque. This significant change in yaw

TABLE 3. Experimental plan for simulation and demonstrator vehicle test drives including both steady-state circular driving maneuvers and double lane change maneuvers combined with different failure scenarios (steering actuator SA_a, drive motor left D_1 or right D_2) as well as modifications in the control allocation setup.

Experiment ID	Maneuver	Failure	Control Allocation Setup
S01_C_δ_fS_noComp	Simulation, circle, $\delta_{ref} = 0.089$ rad, $v_{r,ref} = 8$ m/s	SA_a	Without TV compensation
S02_C_δ_fS	Simulation, circle, $\delta_{ref} = 0.089$ rad, $v_{r,ref} = 8$ m/s	SA_a	Default
S03_C_r_fS	Simulation, circle, $R_{r,ref} = 24$ m, $v_{r,ref} = 8$ m/s	SA_a	Default
S04_C_δ_fD1	Simulation, circle, $\delta_{ref} = 0.089$ rad, $v_{r,ref} = 8$ m/s	D_1	Default
S05_C_δ_fD2	Simulation, circle, $\delta_{ref} = 0.089$ rad, $v_{r,ref} = 8$ m/s	D_2	Default
S11_LC	Simulation, double lane change, $v_{r,ref} = 8$ m/s	-	Default
S12_LC_fS	Simulation, double lane change, $v_{r,ref} = 8$ m/s	SA_a	Default
S13_LC_fD1	Simulation, double lane change, $v_{r,ref} = 8$ m/s	D_1	Default
S14_LC_fD2	Simulation, double lane change, $v_{r,ref} = 8$ m/s	D_2	Default
D11_LC	Demonstrator vehicle, double lane change, $v_{r,ref} = 5.5$ m/s	-	Default
D12_LC_fS	Demonstrator vehicle, double lane change, $v_{r,ref} = 5.5$ m/s	SA_a	Default
D13_LC_fD1	Demonstrator vehicle, double lane change, $v_{r,ref} = 5.5$ m/s	D_1	Default
D14_LC_fD2	Demonstrator vehicle, double lane change, $v_{r,ref} = 5.5$ m/s	D_2	Default

TABLE 4. Evaluation of the simulation and the demonstrator vehicle test drives based on the defined metrics. For the steady-state circular driving maneuvers, these are: maximum and root-mean-square (RMS) steering angle control error ($\delta_{error,max}$ and $\delta_{error,RMS}$), maximum and RMS deviation of the yaw rate compared to the value before failure ($\Delta\dot{\psi}_{max}$ and $\Delta\dot{\psi}_{RMS}$) and maximum and RMS deviation of the crosstrack error compared to the value before failure ($\Delta e_{lat,r_{max}}$ and $\Delta e_{lat,r_{RMS}}$). For the double lane change maneuvers these are: maximum and RMS steering angle control error ($\delta_{error,max}$ and $\delta_{error,RMS}$), maximum and RMS crosstrack error ($e_{lat,r_{max}}$ and $e_{lat,r_{RMS}}$) and minimum distance of the vehicle to the lane boundaries ($d_{lim,min}$).

Experiment ID	$\delta_{error,max}$ (rad)	$\delta_{error,RMS}$ (rad)	$\Delta\dot{\psi}_{max}$ (rad/s)	$\Delta\dot{\psi}_{RMS}$ (rad/s)	$\Delta e_{lat,r_{max}}$ (m)	$\Delta e_{lat,r_{RMS}}$ (m)
S01_C_δ_fS_noComp	1.1×10^{-3}	1.1×10^{-4}	8.67×10^{-2}	77.7×10^{-3}	-	-
S02_C_δ_fS	-7.2×10^{-3}	10.5×10^{-4}	2.28×10^{-2}	5.41×10^{-3}	-	-
S03_C_r_fS	-6.5×10^{-3}	12.6×10^{-4}	4.46×10^{-2}	7.21×10^{-3}	0.58×10^{-2}	0.17×10^{-2}
S04_C_δ_fD1	-6.3×10^{-3}	9.3×10^{-4}	2.20×10^{-2}	4.15×10^{-3}	-	-
S05_C_δ_fD2	6.2×10^{-3}	6.2×10^{-4}	-1.97×10^{-2}	2.41×10^{-3}	-	-
Experiment ID	$\delta_{error,max}$ (rad)	$\delta_{error,RMS}$ (rad)	$e_{lat,r_{max}}$ (m)	$e_{lat,r_{RMS}}$ (m)	$d_{lim,min}$ (m)	
S11_LC	22.0×10^{-3}	87.2×10^{-4}	3.60×10^{-2}	2.05×10^{-2}	3.24×10^{-2}	
S12_LC_fS	-15.9×10^{-3}	70.4×10^{-4}	5.01×10^{-2}	2.92×10^{-2}	3.94×10^{-2}	
S13_LC_fD1	28.7×10^{-3}	96.0×10^{-4}	3.57×10^{-2}	1.91×10^{-2}	2.23×10^{-2}	
S14_LC_fD2	35.0×10^{-3}	103×10^{-4}	3.31×10^{-2}	1.87×10^{-2}	2.49×10^{-2}	
D11_LC	73.4×10^{-3}	314×10^{-4}	5.97×10^{-2}	2.83×10^{-2}	2.32×10^{-2}	
D12_LC_fS	78.2×10^{-3}	300×10^{-4}	6.12×10^{-2}	2.95×10^{-2}	3.30×10^{-2}	
D13_LC_fD1	81.2×10^{-3}	336×10^{-4}	-5.40×10^{-2}	2.87×10^{-2}	3.04×10^{-2}	
D14_LC_fD2	79.7×10^{-3}	336×10^{-4}	6.52×10^{-2}	3.12×10^{-2}	2.82×10^{-2}	

rate, and therefore in lateral vehicle motion, was expected and was the reason for implementing the torque vectoring compensation functionality, which was investigated in the following experiment.

In the second experiment (S02), the reference steering angle was adjusted based on the current differential drive torques with the objective of maintaining the previous yaw rate after the failure event. The reference steering angle decreases from 0.089 to 0.078 (-12%) while the differential drive torque and therefore the induced yaw torque increase, but unlike the previous experiment no overshoot is observed. The actual steering angle follows the corrected reference with a slight delay.

The change in the vehicle's yaw rate after the failure is the result of two opposing effects. On the one hand, the increasing differential torque contributes to an increase in the yaw torque, and on the other hand, the decreasing steering angle reduces the yaw torque. Analysis of the yaw rate shows the effectiveness of the compensation, as the yaw rate peaks at $+6.8\%$, but then smoothly returns to the previous value. After 1.55 s, the deviation is less than 1% of the value before the failure.

It is important to note that an exact return to the pre-failure value was not expected because the yaw rate is not closed-loop controlled and the compensation relies purely on analytically calculated correlation k_{δ,M_z}. Therefore, this result can also confirm the validity of the derivation for torque vectoring compensation and in particular the validity of k_{δ,M_z}.

The initial two experiments were carried out by specifying a constant steering angle input, representing the manual driving scenario with a drive-by-wire system, while the third experiment (S03) was performed using the path tracking controller. This configuration represents an automated or assisted driving scenario. The reference steering angle is therefore not constant, but is dynamically adjusted by the

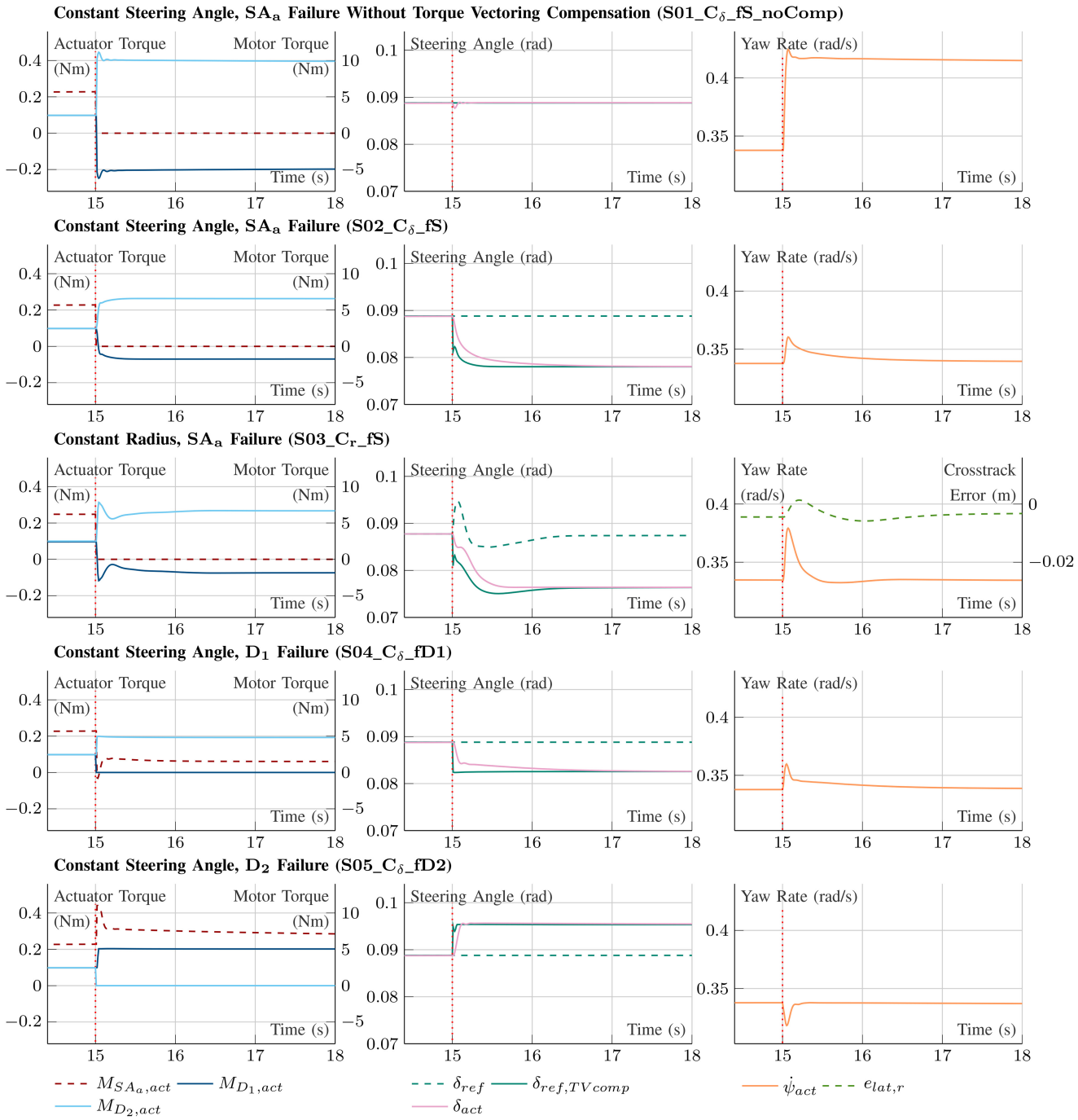

FIGURE 6. Results of the simulated test drives of the steady-state circular driving maneuver (experiment IDs S01-S05) with actuator or motor failure at $t = 15$ s (indicated by the dotted vertical line). For each experiment, the actual actuator and motor torques are plotted (left), complemented by the reference and actual steering angles (center) and the resulting yaw rate and crosstrack error (right).

controller to keep the vehicle on a circular path with a constant radius.

Prior to the failure, the resulting crosstrack error is -0.004 m (note that the path tracking controller used does not completely compensate for steady-state errors). After the failure, the crosstrack error changes by 0.0054 m within 0.2 s and later stabilizes close to the pre-failure value at -0.003 m.

Similar to the previous experiment, the yaw rate reaches a peak in consequence of the failure. With $+13.3\%$ the peak is higher but returns faster to the pre-failure level as before.

The small disturbance of the crosstrack error, despite the significant yaw rate deviation, can be explained by considering the vehicle's dynamic state before and after the failure. When the vehicle moves with its reference point, the center of the rear axle, on the intended radius of the

circle, the orientation of the vehicle is rotated by the slip angle of the rear axle relative to the direction of motion of the reference point. The slip angle is dependent on the lateral force acting on the rear axle (refer to (28)). This force is a result of the difference between the two driving forces on the front axle, as stated by (4). Thus, the vehicle is oriented differently with respect to the direction of motion of the reference point in the steady state before and after the failure, when compensated by differential steering.

This change of orientation $\Delta\alpha_r$ results with (4) and (28) in

$$\Delta\alpha_r = \cos(\delta_{act})\frac{i_{DG}w}{2r_w l C_{y_{3,4}}}\left(M_{D_2,act} - M_{D_1,act}\right). \quad (34)$$

With the parameters of the vehicle and the driving condition before and after the failure, $\Delta\alpha_r$ is found to be 0.00556 rad.

In addition to the vehicle's continuous rotation during circular motion with a constant yaw rate, there is an extra rotation required due to the change in slip angle resulting from differential steering failure compensation. Consequently, this angular difference by which the vehicle is additionally rotated must result in a brief increase in the yaw rate. Integrating the increase in yaw rate measured in experiment S03 during the 3 s post-failure time interval, the resulting angle is 0.00521 rad, which is within 6% of the expected value calculated in (34).

From these considerations, we conclude that a deviation in the yaw rate after the failure is not an undesirable side effect. Rather, it is necessary to make the transition from the use of a steering actuator to differential steering without the vehicle deviating from its course.

With reference to the evaluation of the previous experiment (S02), in which the steering angle position was considered to be constant, it can be concluded that the yaw rate peak observed there is also not to be considered as a deficiency, but as necessary for the vehicle to behave in an uninfluenced manner according to the driver's manual input.

Another conclusion that can be drawn from experiment S03 concerns the path tracking controller. The change of the slip angle on the two axes due to torque vectoring affects the calculations of the control approach, leading to the modifications described in Appendix B. The accurate match of the crosstrack error before and after the failure confirms the effectiveness of these modifications.

In response to the actuator failure, the tracking controller must correct the vehicle guidance by adjusting the output reference steering angle. The steering angle is briefly increased and subsequently reduced relative to the prior and later stationary state. This behavior can also be explained by the increase in the slip angle of the rear axle, resulting in additional rotation of the vehicle around its center of gravity. This causes the rear axle to follow a larger radius than before, on the right side of the path. To realign the reference point with the intended path, the steering angle must be adjusted first to the left and then to the right, similar to the sequence of a lane change maneuver, but with a very small offset. Experiments S04 and S05 considered the failure of a drive motor while driving at a constant steering angle. After the failure, the drive torque of the intact drive results directly from the required total drive torque. The steering torque to be applied by the steering actuator is composed of the required steering torque and the amount caused by differential steering due to the one-sided drive failure. If the inner drive fails (S04), the operating outer drive will assist the steering actuator so that the actuator torque is reduced from 0.23 Nm to 0.06 Nm. Due to the torque vectoring effect, the steering angle must be reduced, which occurs immediately after the failure and results in a brief negative steering torque.

In case of the failure of the outer drive (S05), the steering actuator torque initially increases sharply after the failure because the steering angle must be increased, and remains at a higher level than before the failure because the remaining drive torque counteracts the steering torque. In this case, the yaw rate briefly changes in a negative direction because the sideslip angle at which the vehicle is moving is reduced as a result of the failure.

These results indicate that despite the effect on steering torque, the proposed approach can also compensate for the failure of a drive in the intended way.

2) DOUBLE LANE CHANGE

The evaluation of the double lane change experiments serves to verify whether the findings from the steady-state circular driving maneuvers also apply to a challenging driving situation with rapidly changing dynamics.

Fig. 7 compares the results of the double lane change with steering actuator failure (experiment S12) with those of the experiment without failure (S11, dashed lines).

The graphs of the drive torques demonstrate the functionality of the modified path tracking controller, which outputs a reference torque vectoring differential torque in addition to the steering angle. This results in different right and left drive torques to support the yaw motion of the vehicle in the non-failure case. This also proves that the control allocation accurately meets this secondary objective while still satisfying the higher priority primary objectives (drive torque and steering torque).

The RMS crosstrack error of the non-failure reference experiment of the double lane change maneuver is 0.0205 m, and the closest approach to the lane boundaries is 0.0324 m (see Table 4).

After the steering actuator failure (experiment S12), the required differential torque builds up and simultaneously the compensated reference steering angle decreases until the differential torque briefly reaches its maximum, which is limited by the maximum adjustable drive torques. The maximum possible differential torque is set, therefore the required total drive torque must be neglected. This is intentional since the weighting factors prioritize lateral guidance over longitudinal guidance.

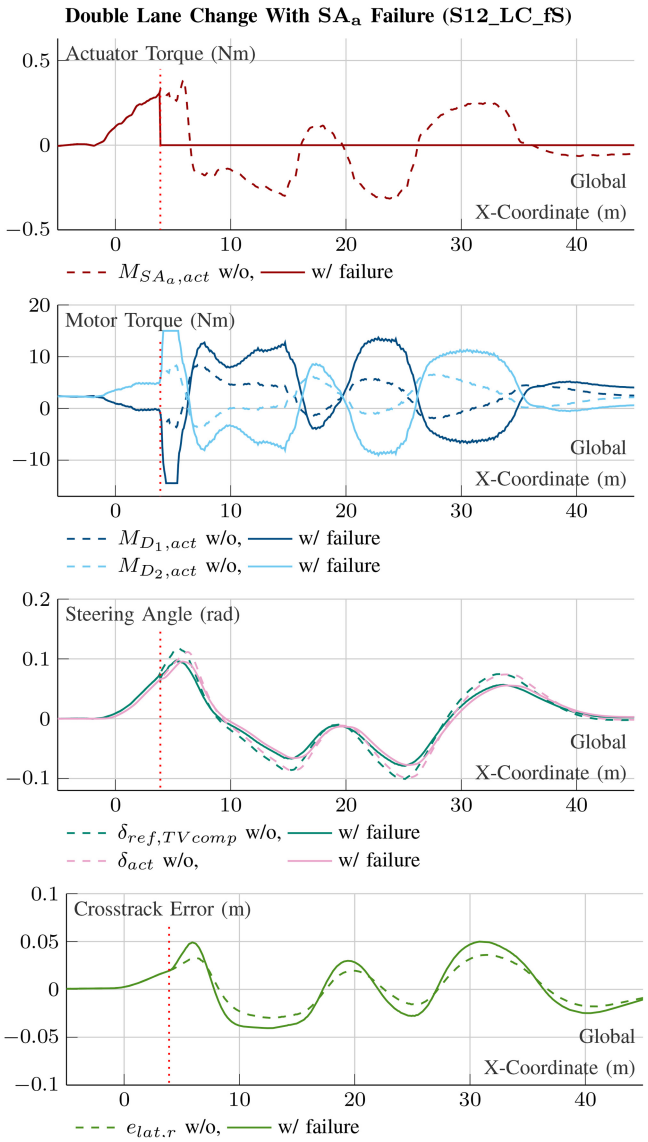

FIGURE 7. Results of the simulated test drives of the double lane change maneuver without and with actuator failure (experiment IDs S11 and S12). The actual actuator and motor torques are plotted, along with the reference and actual steering angles and the resulting crosstrack error. The position of the actuator failure is indicated by the dotted vertical line.

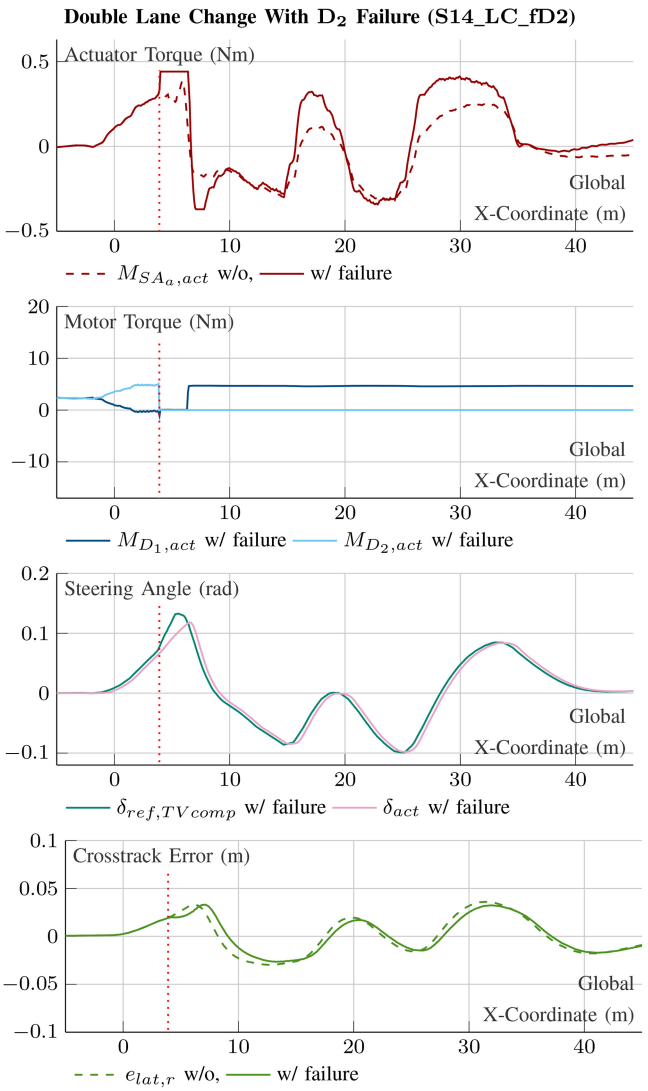

FIGURE 8. Results of the simulated test drives of the double lane change maneuver without and with drive motor failure (experiment IDs S11 and S14). The actual actuator and motor torques are plotted, along with the reference and actual steering angles and the resulting crosstrack error. The position of the actuator failure is indicated by the dotted vertical line.

Near its four peaks, the compensated reference steering angle consistently has a smaller magnitude compared to the non-failure experiment. This is because the torque vectoring effect from differential steering supports the desired yaw motion in these sections. Consequently, the torque vectoring compensation adjusts the steering angle accordingly. The total RMS error of the steering angle controller is 0.00704 rad, and therefore even smaller than in the non-failure experiment (0.00872 rad). Although the RMS crosstrack error of 0.0501 m is larger than in the non-failure scenario, the maneuver can still be performed safely, with the minimum distance to the lane boundaries of 0.039 m remaining even larger than in the non-failure case.

To conclude the analysis of the simulation study, the experiment with the failure of the right drive motor (Fig. 8) is discussed next.

In case of a failure of the right drive, the left drive torque is determined by the constant total drive torque setpoint. This leads to a constant differential torque that must be compensated for by a positive steering actuator torque offset. The offset can be observed by comparing the steering actuator torque profiles for the case with and without drive failure in the first diagram of Fig. 8. The offset towards larger positive steering actuator torques causes the steering actuator to reach its torque limit directly after the drive failure. As the steering function has priority over the drive function, this results in the drive torque target being violated when the steering actuator limit is reached. This can be

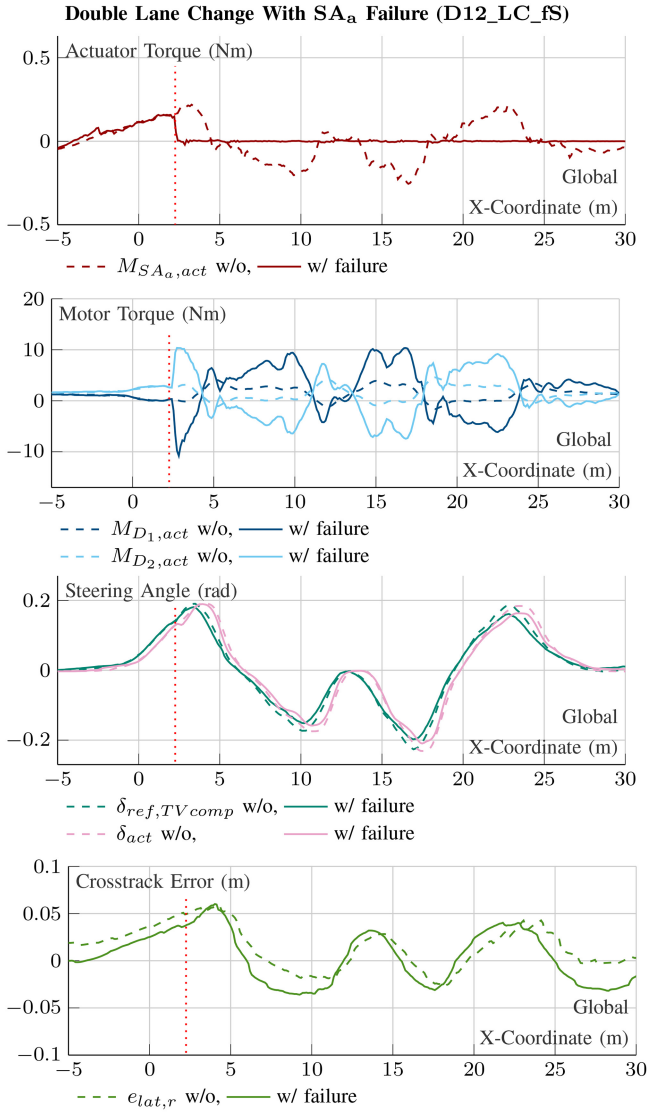

FIGURE 9. Results of demonstrator vehicle test drives of the double lane change maneuver without and with actuator failure (experiment IDs D11 and D12). The actual actuator and motor torques are plotted, along with the reference and actual steering angles and the resulting crosstrack error. The position of the actuator failure is indicated by the dotted vertical line.

observed immediately after the right drive fails and the left drive torque is reduced to approximately 0 Nm.

Overall, the drive failure and its compensation only have a minor impact on the vehicle guidance, as shown by the resulting RMS crosstrack error of 0.0187 m, which is slightly lower than that of the non-failure experiment.

D. DEMONSTRATOR VEHICLE TEST DRIVE RESULTS

Driving tests were conducted with the demonstrator vehicle to verify the approach under real-world conditions (see also the accompanying video in [33]). In order to validate the results of the simulation study, the double lane change experiments are analyzed in the following section. In Fig. 9 the double lane change maneuver without and with actuator failure is compared.

The courses of the actuator torques are qualitatively comparable to those from the simulation study and demonstrate the intended functionality of the control allocation approach in the event of an actuator failure. The transition from using the steering actuator to using differential steering occurs immediately, ensuring uninterrupted lateral control of the vehicle and allowing the maneuver to continue successfully. As shown in Table 4, the vehicle does not approach the lane boundaries closer than 0.0330 m (0.0232 m without failure). The crosstrack error plot indicates no significant increase that would impair safe vehicle control due to the steering actuator failure. The maximum crosstrack error of 0.0612 m in the maneuver with actuator failure is only marginally larger than in the maneuver without failure (0.0597 m). The RMS deviation from the desired path during the lane change is only 0.0295 m (0.0283 m without failure) despite the actuator failure and use of differential steering, which is comparable to the simulation results. In the experiments with the failure of one of the drives, the vehicle does not approach the lane boundaries more closely and shows comparable control performance.

Due to the reduced velocity and therefore the shorter length of the double lane change maneuver compared to the simulation experiment, approximately twice as large steering angle setpoints are required. The deviation between the setpoint and actual steering angles is significantly larger than in the simulation study. While the deviations in the simulation for various failure scenarios ranged between 0.0159 rad and 0.0350 rad, they reach values of 0.0734 rad to 0.0812 rad in the demonstrator vehicle driving tests. The RMS steering angle error increases even more significantly, being on average 3.6 times larger in the demonstrator vehicle tests. A detailed examination of the steering angle profiles during the maneuver indicates that the deviations between the desired and actual steering angles are most significant immediately following the direction changes, and then gradually diminish in the subsequent phase. This phenomenon can be attributed to the friction and the associated high breakaway torque of the vehicle's steering system. A change in the direction of rotation leads to an opposite effect of resistance, requiring the steering torque to initially exceed a certain threshold before an effective steering movement occurs.

Despite this additional challenge compared to the simulated environment, the control approach used can robustly follow the desired steering angle profile, regardless of whether the downstream control allocation provides steering torque through the steering actuator or through differential steering. Combined with the torque vectoring compensation functionality and the consideration of the torque vectoring effect in the vehicle control system, this results in safe vehicle guidance.

Overall, the results of the driving tests with the demonstrator vehicle align with the findings of the simulation study. It can be concluded that the correlations applied in the control effectiveness matrix, the functionality of the

torque vectoring compensation, and the modifications made to account for the torque vectoring effect in the path tracking controller are valid. Moreover, the approach presented has been demonstrated to be effective when applied in a real vehicle environment.

IV. CONCLUSION AND OUTLOOK

With this work, we have demonstrated that differential steering can be employed as cross-actuator redundancy while ensuring a safe and stable transition from nominal to redundant steering control.

The control allocation approach ensures that the upstream longitudinal and lateral controllers are able to guide the vehicle in a stable manner, irrespective of whether steering is achieved through a steering actuator or differential steering. The control allocation prioritizes the steering functionality, thereby also compensating for drive failures without affecting the steering performance. Furthermore, the approach provides an interface for external torque vectoring inputs, which can be considered in failure-free operation if sufficient degrees of freedom are available. The modular design of the approach allows for integration into diverse cascaded control structures and adaptation to a range of vehicle configurations (e.g., four-wheel drive).

A comprehensive examination of the vehicle's dynamics following the actuator failures reveals that the vehicle's behavior remains consistent post-failure, exhibiting no safety-critical deviations from the intended motion. This is observed regardless of whether the driver employs manual steer-by-wire input or the vehicle is steered automatically.

However, an ideally imperceptible transition is not achievable with the vehicle configuration under consideration, as the use of differential steering invariably affects the slip angle, resulting in adjustments to the vehicle's orientation and, consequently, a temporary change in yaw rate.

Overall, the findings confirm the feasibility of using differential steering as cross-actuator redundancy in the event of a steering actuator failure in steer-by-wire systems. However, there are aspects that require further investigation in future research to clarify open questions and to gain a full understanding of the limitations of the approach. Some of these aspects are discussed below:

To incorporate the proposed approach as a redundancy concept in a vehicle, integration into a suitable overall vehicle architecture is required. This architecture could potentially be based on the concept suggested by Bergmiller [4]. In the broader context, it is necessary to identify the vehicle's specifications within its operational domain to derive specific requirements for redundancy, while taking into consideration the existing interactions between its components. This allows the developed concept to be evaluated in terms of functional safety and different configurations of the redundancy concept to be compared.

The control allocation approach could be further developed by introducing the ability to dynamically adjust its parameters, especially the elements of the weighting matrices, depending on the driving situation or actuator states. For instance, an actuator in danger of overheating could be spared. As the control allocation approach relies on the input of an actuator state detection module, the response time requirements for the fault detection function must be derived to define the requirements for such a diagnostic module.

In our study, we focus on the transition from nominal operation to redundant operation, which is particularly applicable in the context of permanent failures. However, in the case of temporary failures, a sudden or intermittent return to nominal operation may occur, resulting in a transition in the opposite direction. In order to prevent this, a component that has failed can be placed into a safe state. If the component recovers fully, the transition back to nominal operation can be initiated in a controlled manner, allowing it to occur under conditions that are not critical from a vehicle dynamics standpoint. Additionally, further studies could investigate the opposite transition in a similar manner.

In order to comprehensively assess the viability of differential steering in general, and the proposed approach in particular, further experiments with real vehicles are necessary. These should provide the evaluation of performance under critical conditions, thereby enabling the identification of limitations. One aspect involves higher velocities, where vehicle stability must be ensured. In the presented cascaded approach, stability arises from the interaction of the various control layers and the additional feedback from the control allocation. This must be tested and optimized for specific configurations.

A further limitation arises in critical driving situations with reduced road adhesion. In such instances, limitations are anticipated that are not derived from the particular implementation of the differential steering control approach. Instead, they represent a general restriction associated with differential steering redundancy. This is because the maximum achievable tire force limits the combined force of longitudinal and lateral forces on the tire. A reduction in adhesion coefficient can significantly diminish the maximum transferable force.

In the context of conventional redundancy with a redundant steering actuator, in the optimal scenario, no longitudinal force is necessary at the tire, thereby allowing the full adhesion potential to be utilized for the generation of lateral force. In contrast, differential steering requires the presence of longitudinal forces at the wheel in order to generate the requisite steering torque, which in turn counteracts the lateral force. Consequently, the maximum attainable lateral force in this scenario is diminished, as a fraction of the available maximum tire force is necessary to generate the requisite longitudinal force. This consequence is partially mitigated by the fact that, according to (4), torque vectoring results in a reduction of the required lateral force at the front axle. Nevertheless, the total tire force required to generate the necessary lateral force remains greater than that which would be required in a scenario using conventional redundancy with a redundant steering actuator. If a maneuver

TABLE 5. Demonstrator vehicle specifications and vehicle model and controller parameters.

Parameter	Description	Value
l	Wheelbase	2.070 m
w	Track width	1.084 m
a	Distance center of gravity to front axle	0.910 m
b	Distance center of gravity to rear axle	1.160 m
m	Mass	394.4 kg
$C_{y_{1,2}}$	Cornering stiffness front wheel pair	28 kN/rad
$C_{y_{3,4}}$	Cornering stiffness rear wheel pair	26 kN/rad
r_W	Dynamic wheel radius	0.2395 m
r_L	Lateral force arm	0.053 m
r_D	Interfering force arm	0.076 m
δ_{max}	Steering angle range	±0.397 rad
i_S	Steering ratio at δ_{center}	393.8
	at δ_{max}	378.0
i_{DG}	Drive motor gear ratio	16
b_{DS}	Differential steering factor	6.00
b_{TV}	TV factor at δ_{center}	36.21
	at δ_{max}	33.39
k_{δ,M_z}	TV compensation factor at δ_{center}	6.84×10^{-5}
	at δ_{max}	7.12×10^{-5}
k	Path tracking crosstrack error param.	$3.5\,\mathrm{s}^{-1}$
$k_{d,yaw}$	Path tracking yaw parameter	0.05 s
t_{ff}	Path tracking feedforward time	0.1 s
$M_{SA,nom}$	Steering actuator nominal torque range	±0.45 Nm
$M_{S,nom}$	Steering torque range at δ_{center}	±177.2 Nm
	at δ_{max}	±170.1 Nm
$M_{D,nom}$	Drive motor torque range (due to slip)	±15 Nm
$F_{long,nom}$	Drive force range	±2004 N
$M_{z,TV_{nom}}$	TV yaw torque range at δ_{center}	±1086 Nm
	at δ_{max}	±1002 Nm

utilizing conventional redundancy already fully exploits the potential of tire force due to reduced adhesion, the use of differential steering is expected to result in lower lateral forces and therefore a larger cornering radius.

To quantify this effect, further experiments could be conducted using a double lane change maneuver at progressively decreasing adhesion levels. This would help identify the adhesion threshold below which redundancy through differential steering does not provide a safe and comparable solution to conventional redundancy.

APPENDIX A
VEHICLE SPECIFICATIONS

Specifications of the demonstrator vehicle and its components, as well as the resulting torque ranges and vehicle control parameters, are listed in Table 5.

APPENDIX B
MODIFIED PATH TRACKING CONTROLLER

A. CONSIDERING DRIVE TORQUES IN THE CONTROL APPROACH

The basis for the path tracking controller used is the enhanced Stanley controller by Seiffer et al. [22]. The modifications made to account for the influence of longitudinal forces and torque vectoring are described below. The corresponding equations in [22] are referenced.

When calculating $\theta_{ss,f_{long}}$ and $\theta_{ss,r_{mod}}$ (refer to equations [22, eqs. (14) and (15)]), it is necessary to consider the influence of the total drive force F_{long} on the slip angles.

According to Römer [5] the additional yaw torque $M_{z,long}$ caused by the total drive forces is given by

$$M_{z,long} = \left(F_{W_1,long} + F_{W_2,long}\right)\sin(\delta_{act})a \tag{35}$$

and its effect on the lateral forces by

$$\begin{aligned}\Delta F_{W_{1,2},lat} &= -\frac{M_{z,long}}{\cos(\delta_{act})l}\\ \Delta F_{W_{3,4},lat} &= \frac{M_{z,long}}{l}.\end{aligned} \tag{36}$$

Thus $\theta_{ss,f_{mod}}$ and $\theta_{ss,r_{mod}}$ result in

$$\begin{aligned}\theta_{ss,f_{mod}} &= \theta_{ss,f} - \frac{\tan(\delta_{act})a}{lC_{y_{1,2}}}F_{long}\\ \theta_{ss,r_{mod}} &= \theta_{ss,r} + \frac{\sin(\delta_{act})a}{lC_{y_{3,4}}}F_{long}.\end{aligned} \tag{37}$$

Further effects caused by the torque vectoring error $M_{z,TV_{error}}$ must be taken into account in the control law. It must be ensured that the effects already taken into account in the TV compensation (Section II-C3) are not compensated twice.

The vehicle orientation to be expected in the steady state is influenced by $M_{z,TV_{error}}$. The resulting angle $\theta_{ss,r_{TV}}$ is given in analogy to (4) by

$$\theta_{ss,r_{TV}} = \frac{1}{C_{y_{3,4}}l}M_{z,TV_{error}}. \tag{38}$$

The angle $\theta_{ss,r_{TV}}$ must be considered in different equations as follows.

The reference coordinates of the front axis $x_{f,ref}$ and $y_{f,ref}$ (see [22, eq. (4)]) become

$$\begin{aligned}x_{f,ref_{mod}} &= x_{r,ref} + l\cos\big(\psi_{r,ref}\\ &\quad + \theta_{ss,r_{mod}} + \theta_{ss,r_{TV}}\big)\\ y_{f,ref_{mod}} &= y_{r,ref} + l\sin\big(\psi_{r,ref}\\ &\quad \theta_{ss,r_{mod}} + \theta_{ss,r_{TV}}\big).\end{aligned} \tag{39}$$

Accordingly, the kinematic reference steering angle $\delta_{\kappa,ref}$ and the reference orientation $\psi_{f,ref}$ ([22, eqs. (7) and (8)]) become

$$\delta_{\kappa,ref_{mod}} = \arctan\frac{l\kappa_{ref} - \sin\big(\theta_{ss,r_{mod}} + \theta_{ss,r_{TV}}\big)}{\cos\big(\theta_{ss,r_{mod}} + \theta_{ss,r_{TV}}\big)}, \tag{40}$$

$$\psi_{f,ref_{mod}} = \psi_{r,ref} + \theta_{ss,r_{mod}} + \theta_{ss,r_{TV}} + \delta_{\kappa,ref_{mod}}, \tag{41}$$

and the actual orientation error θ_r^* (equation (17) in [22])

$$\theta^*_{r,mod} = \psi_{r,ref} - \psi_r + \theta_{ss,r_{mod}} + \theta_{ss,r_{TV}}. \tag{42}$$

B. TORQUE VECTORING REFERENCE CALCULATION

The purpose of the torque vectoring approach used is not to obtain an optimal torque vectoring reference, but to provide a simple and robust solution that proves that the proposed control allocation method can handle this additional input. Therefore, a simple technique is implemented to compute the torque vectoring reference $M_{z,TV_{ref}}$.

In the first step the path tracking controller's steering angle output δ_{ref} is taken to calculate a corresponding yaw rate target $\dot{\psi}_{ref}$. By considering the bicycle model and eliminating the slip angle-related effects within δ_{ref} (refer to equations (5), (7), and (13) in [22]), we obtain

$$\dot{\psi}_{ref} = \frac{v_{r,act}}{l}\left(\tan\left(\delta_{ref} - \theta_{ss,f_{mod}}\right)\cos\left(\theta_{ss,r_{mod}}\right) + \sin\left(\theta_{ss,f_{mod}}\right)\right). \tag{43}$$

In the second step, the target torque vectoring torque is calculated based on the difference between the reference and the actual yaw rate. This yields

$$M_{z,TV_{ref}} = kp_{yaw}\left(\dot{\psi}_{ref} - \dot{\psi}_{act}\right). \tag{44}$$

The parameter kp_{yaw} can be used to adjust the intensity of the torque vectoring support. A value of 10000 was chosen to observe appropriate behavior.

ACKNOWLEDGMENT

The authors would like to thank Alejandra Castillo, Luca Wahl, Timo Lorenz, and Clemens Brauch for their contributions to this research as part of their theses and working student projects.

REFERENCES

[1] M. Hales and K. Pattok, "Safety standards for steer-by-wire systems," in *Proc. 12th Int. Munich Chassis Symp.*, 2022, pp. 675–692. [Online]. Available: https://doi.org/10.1007/978-3-662-64550-5_38

[2] J. Becker, M. Helmle, and O. Pink, *System Architecture and Safety Requirements for Automated Driving*. Cham, Switzerland: Springer, 2016, pp. 265–283. [Online]. Available: https://doi.org/10.1007/978-3-319-31895-0_11

[3] C. Huang, F. Naghdy, H. Du, and H. Huang, "Fault tolerant steer-by-wire systems: An overview," *Annu. Rev. Control*, vol. 47, pp. 98–111, Jan. 2019. [Online]. Available: https://doi.org/10.1016/j.arcontrol.2019.04.001

[4] P. J. Bergmiller, *Towards Functional Safety in Drive-by-Wire Vehicles*. Cham, Switzerland: Springer, 2015. [Online]. Available: https://doi.org/10.1007/978-3-319-17485-3

[5] J. Römer, "Steuerung und Regelung des Lenkradmoments durch Nutzung radselektiver Frontantriebe," Ph.D. dissertation, Instit. Veh. Syst. Technol., Karlsruhe Inst. Technol. (KIT), Karlsruhe, Germany, Jan. 2022. [Online]. Available: https://doi.org/10.5445/ksp/1000132577

[6] Q. Li, X. li Yu, H. Zhang, and R. Huang, "Study on differential assist steering system with double in-wheel motors with intelligent controller," *Math. Problems Eng.*, vol. 2015, pp. 1–8, Dec. 2015. [Online]. Available: https://doi.org/10.1155/2015/910230

[7] J. Wang, Q. Wang, and L. Jin, "Modeling and simulation studies on differential drive assisted steering for EV with four-wheel-independent-drive," in *Proc. IEEE Veh. Power Propuls. Conf.*, 2008, pp. 1–7. [Online]. Available: https://doi.org/10.1109/vppc.2008.4677428

[8] A. D. Dominguez-Garcia, J. G. Kassakian, and J. E. Schindall, "A backup system for automotive steer-by-wire, actuated by selective braking," in *Proc. IEEE 35th Annu. Power Electron. Spec. Conf.*, 2004, pp. 383–388. [Online]. Available: https://doi.org/10.1109/pesc.2004.1355774

[9] M. Jonasson and M. Thor, "Steering redundancy for self-driving vehicles using differential braking," *Veh. Syst. Dyn.*, vol. 56, no. 5, pp. 791–809, May 2018. [Online]. Available: https://doi.org/10.1080/00423114.2017.1356929

[10] C. Hu et al., "Lane keeping of autonomous vehicles based on differential steering with adaptive multivariable super-twisting control," *Mech. Syst. Signal Process.*, vol. 125, pp. 330–346, Jun. 2019. [Online]. Available: https://doi.org/10.1016/j.ymssp.2018.09.011

[11] K. Polmans, "Torque vectoring as redundant steering for automated driving or steer-by-wire," in *Proc. 5th Int. Munich Chassis Symp.*, 2014, pp. 163–177. [Online]. Available: https://doi.org/10.1007/978-3-658-05978-1_13

[12] J. Tian, Q. Wang, J. Ding, Y. Wang, and Z. Ma, "Integrated control with DYC and DSS for 4WID electric vehicles," *IEEE Access*, vol. 7, pp. 124077–124086, 2019. [Online]. Available: https://doi.org/10.1109/access.2019.2937904

[13] C. Hu, R. Wang, F. Yan, Y. Huang, H. Wang, and C. Wei, "Differential steering based yaw Stabilization using ISMC for independently actuated electric vehicles," *IEEE Trans. Intell. Transp. Syst.*, vol. 19, no. 2, pp. 627–638, Feb. 2018. [Online]. Available: https://doi.org/10.1109/TITS.2017.2750063

[14] M. Kuslits, "Analysis and optimisation of a new differential steering concept," Ph.D. dissertation, Chair Eng. Mech. Veh. Dyn., Brandenburg Univ. Technol., Cottbus, Germany, Dec. 2022. [Online]. Available: https://doi.org/10.30819/5578

[15] A. Seiffer, L. Schütz, M. Frey, and F. Gauterin, "Constrained control allocation improving fault tolerance of a four wheel independently driven articulated vehicle," *IEEE Open J. Intell. Transp. Syst.*, vol. 4, pp. 187–203, 2023. [Online]. Available: https://doi.org/10.1109/ojits.2023.3252399

[16] T. Stolte, "Actuator fault-tolerant vehicle motion control: A survey," 2021, *arXiv:2103.13671*. [Online]. Available: https://doi.org/10.48550/arXiv.2103.13671

[17] M. Eckert, "Energieoptimale Fahrdynamikregelung mehrmotoriger Elektrofahrzeuge," Ph.D. dissertation, Instit. Veh. Syst. Technol., Karlsruhe Inst. Technol. (KIT), Karlsruhe, Germany, Oct. 2014. [Online]. Available: https://doi.org/10.5445/ksp/1000045234

[18] C. Knobel, A. Pruckner, and T. Bünte, "Optimized force allocation: A general approach to control and to investigate the motion of over-actuated vehicles," *IFAC Proc. Vol.*, vol. 39, no. 16, pp. 366–371, 2006. [Online]. Available: https://doi.org/10.3182/20060912-3-DE-2911.00065

[19] P. Kautzmann, M. Frey, J. Römer, M. Götz, and M. P. Mayer, *Energieoptimale, intelligente Lenkkraftunterstützung für elektrische Fahrzeuge (e^2-Lenk)*, Karlsruhe Inst. Technol. (KIT), Karlsruhe, Germany, 2018. [Online]. Available: https://doi.org/10.2314/GBV:1049069447

[20] P. Kautzmann, "Entwicklungsmethodik für Fahrwerke in Fahrzeugen mit Lenkkraftunterstützung durch radselektive Antriebe," Ph.D. dissertation, Instit. Veh. Syst. Technol., Karlsruhe Inst. Technol. (KIT), Karlsruhe, Germany, 2023. [Online]. Available: https://doi.org/10.5445/IR/1000165608

[21] J. Kolb et al., *SmartLoad—Neue Methoden zur Zuverlässigkeitssteigerung von hochautomatisierten elektrischen Fahrzeugen; Verfahren zur Fehlertoleranz und Redundanzmanagment auf Aktor- und Systemebene: Schaeffler Technologies*. Karlsruhe Inst. Technol. (KIT), Karlsruhe, Germany, 2022. [Online]. Available: https://doi.org/10.2314/KXP:1845896122

[22] A. Seiffer, M. Frey, and F. Gauterin, "Pragmatic and effective enhancements for Stanley path-tracking controller by considering system delay," *Vehicles*, vol. 5, no. 2, pp. 615–636, May 2023. [Online]. Available: https://doi.org/10.3390/vehicles5020034

[23] A. Seiffer, S. Li, and T. Schulz, *Vehicle Dynamics Model of Demonstrator Vehicle 'elf++'*, Karlsruhe Inst. Technol. (KIT), Karlsruhe, Germany, 2023. [Online]. Available: https://doi.org/10.5445/ir/1000154571

[24] *IPG Automotive Group CarMaker Programmer'S Guide Version 8.0*, IPG Automot. Group, Karlsruhe, Germany, 2019.

[25] A. Seiffer, *Radselektive Antriebe als Redundanz des Lenkaktors*, Karlsruhe Inst. Technol. (KIT), Karlsruhe, Germany, 2023. [Online]. Available: https://doi.org/10.5445/ir/1000159300

[26] G. Reiter, K. Pohlmans, C. Miano, A. Hackl, and C. Lex, "Suspension influences on a steer-by-wire torque vectoring vehicle," in *Proc. 18. Int. Stuttgarter Symp.*, 2018, pp. 327–341. [Online]. Available: https://doi.org/10.1007/978-3-658-21194-3_27
[27] M. W. Oppenheimer, D. B. Doman, and M. A. Bolender, "Control allocation for over-actuated systems," in *Proc. 14th Mediterr. Conf. Control Autom.*, 2006, pp. 1–6. [Online]. Available: https://doi.org/10.1109/med.2006.328750
[28] S. Li, M. Frey, and F. Gauterin, "Evaluation of different fault diagnosis methods and their applications in vehicle systems," *Machines*, vol. 11, no. 4, p. 482, Apr. 2023. [Online]. Available: https://doi.org/10.3390/machines11040482
[29] O. Härkegård, "Efficient active set algorithms for solving constrained least squares problems in aircraft control allocation," in *Proc. 41st IEEE Conf. Decis. Control*, 2002, pp. 1295–1300. [Online]. Available: https://doi.org/10.1109/cdc.2002.1184694
[30] (MathWorks Inc., Natick, MA, USA). *Active-Set Quadprog Algorithm*. Accessed: Jun. 24, 2023. [Online]. Available: https://de.mathworks.com/help/optim/ug/quadratic-programming-algorithms.html?#mw%5Fb973f7d7-646c-486a-b04a-cf049a38cb92
[31] *Road Vehicles—Lateral Transient Response Test Methods—Open-Loop Test Methods*, ISO Standard 7401:2011, 2011. [Online]. Available: https://www.iso.org/standard/54144.html
[32] *Passenger Cars—Test Track for a Severe Lane-Change Manoeuvre—Part 1: Double Lane-Change*, ISO Standard 3888-1:2018, 2018. [Online]. Available: https://www.iso.org/standard/67973.html
[33] A. Seiffer and T. Schulz, *Demonstrator Vehicle Compensating for Steering Actuator Failure by Differential Steering*, Sep. 2023. [Online Video]. Available: https://doi.org/10.5445/IR/1000161921

ALEXANDER SEIFFER received the M.Sc. degree in mechanical engineering from the Karlsruhe Institute of Technology (KIT), Karlsruhe, Germany, in 2015. He is currently pursuing the Doctoral degree in the Working Group Automated Mobility with the Schaeffler SHARE at KIT (Schaeffler Hub for Advanced Research at Karlsruhe Institute of Technology). Since 2015, he has been working with Schaeffler Technologies AG & Co. KG, Supervised by Frank Gauterin. His research interests include automated driving, technical reliability and resilience, vehicle dynamics, and over-actuated vehicles.

MICHAEL FREY received the Diploma and Doctoral degrees in mechanical engineering from the University of Karlsruhe in 1993 and 2004, respectively. He is the Manager of the Research Group Automation and the Research Group Suspension and Propulsion Systems, Institute of Vehicle System Technology. His research interests are autonomous driving, driver assistance systems, operational strategies, suspension systems, vehicle dynamics, as well as vehicle modeling and optimization.

FRANK GAUTERIN received the Diploma degree in physics from the University of Münster, Germany, in 1989, and the Dr.rer.nat. (Ph.D.) degree from the University of Oldenburg, Germany, in 1994. From 1989 to 2000, he worked as an Acoustics Engineer and from 2000 to 2006 as the Director of the Noise Vibration and Harshness Engineering Profit Centre, Continental AG, Hanover, Germany, with locations in Germany, USA, and Malaysia. From 2006 to 2024, he was a Full Professor of Vehicle Technology with the Karlsruhe Institute of Technology (KIT), Germany, the Head of the Institute of Vehicle System Technology, and a Scientific Spokesperson with KIT Centre Mobility Systems. His research interests are vehicle conception, control, suspension and drive systems, tire road interaction, and NVH.